The Role of Radiative Interactions in Tropical Cyclone Development under Realistic Boundary Conditions

BOSONG ZHANG,[a] BRIAN J. SODEN,[a] GABRIEL A. VECCHI,[b,c] AND WENCHANG YANG[b]

[a] *Rosenstiel School of Marine and Atmospheric Science, University of Miami, Miami, Florida*
[b] *Department of Geosciences, Princeton University, Princeton, New Jersey*
[c] *High Meadows Environmental Institute, Princeton University, Princeton, New Jersey*

(Manuscript received 22 July 2020, in final form 4 December 2020)

ABSTRACT: The impact of radiative interactions on tropical cyclone (TC) climatology is investigated using a global, TC-permitting general circulation model (GCM) with realistic boundary conditions. In this model, synoptic-scale radiative interactions are suppressed by overwriting the model-generated atmospheric radiative cooling rates with their monthly varying climatological values. When radiative interactions are suppressed, the global TC frequency is significantly reduced, indicating that radiative interactions are a critical component of TC development even in the presence of spatially varying boundary conditions. The reduced TC activity is primarily due to a decrease in the frequency of pre-TC synoptic disturbances (''seeds''), whereas the likelihood that the seeds undergo cyclogenesis is less affected. When radiative interactions are suppressed, TC genesis shifts toward coastal regions, whereas TC lysis locations stay almost unchanged; together the distance between genesis and lysis is shortened, reducing TC duration. In a warmer climate, the magnitude of TC reduction from suppressing radiative interactions is diminished due to the larger contribution from latent heat release with increased sea surface temperatures. These results highlight the importance of radiative interactions in modulating the frequency and duration of TCs.

KEYWORD: Tropical cyclones

1. Introduction

Convective aggregation has been extensively studied in idealized numerical simulations, in which randomly distributed convective systems can spontaneously organize into one or several isolated clusters under highly idealized boundary conditions. Previous studies have demonstrated that radiative feedbacks can play an important role in the development of organized convection (Bretherton et al. 2005; Emanuel et al. 2014; Holloway and Woolnough 2016; Muller and Bony 2015; Muller and Held 2012; Wing and Emanuel 2014; Wing et al. 2016). Typically, the impact of radiative feedbacks is assessed by performing mechanism-denial experiments in which radiative feedbacks are turned off by prescribing fixed radiative cooling rates, thus disabling interactions between radiation and convection. Using this approach, it has been shown that homogenizing longwave radiative cooling can prevent convective aggregation regardless of the domain size or horizontal resolution in a cloud-resolving model (Muller and Held 2012). Yang (2018) showed that homogenizing radiative cooling in the boundary layer can also inhibit the aggregation process. Physically, the spatial variability of radiative cooling plays an important role in generating a secondary low-level circulation and producing an upgradient moist static energy (MSE) transport (Muller and Bony 2015; Muller and Held 2012; Wing and Emanuel 2014), which is thought to be a key positive feedback in the aggregation process (Bretherton et al. 2005).

Idealized numerical models are useful tools to study the relationship between radiative feedbacks and convective aggregation. However, various assumptions are usually made in idealized simulations such as uniform sea surface temperatures (SSTs), no wind shear, and no rotation. In the real world, the impact of SST gradients or wind shear may overwhelm the feedbacks involved in generating convective aggregation under idealized settings. Thus, the importance of these feedbacks in generating convective aggregation in the real atmosphere remains unclear. To close the gap between convection simulated in idealized models and that in the real world, the impact of radiative feedbacks on convective aggregation should be assessed under more realistic boundary conditions provided by GCMs.

Previous studies using GCMs have mostly examined the impact of radiative changes induced by clouds by making clouds transparent to radiation. Early studies have shown that cloud radiative effects (CRE) can influence convection, precipitation, and the general circulation (Randall et al. 1989; Sherwood et al. 1994; Slingo and Slingo 1988). In the tropics, Fermepin and Bony (2014) revealed that radiative effects of low clouds enhance tropical precipitation and circulation through their coupling to surface fluxes. The CRE also modifies internal modes of tropical variability such as the Madden–Julian oscillation (Crueger and Stevens 2015). In the extratropics,

Supplemental information related to this paper is available at the Journals Online website: https://doi.org/10.1175/JCLI-D-20-0574.s1.

Corresponding author: Bosong Zhang, bosong.zhang@rsmas.miami.edu

Publisher's Note: This article was revised on 19 February 2021 to correct typographical errors in Eq. (8) and following text that were introduced during the production process.

DOI: 10.1175/JCLI-D-20-0574.1

the CRE acts to increase the meridional temperature gradient and strengthen the midlatitude jet (Li et al. 2015). Some of these studies have used output from the Clouds On-Off Klimate Intercomparison Experiment (COOKIE) project (Stevens et al. 2012), which compares simulations with clouds that are transparent to radiation (clouds off) and those including the CRE (clouds on).

Convective aggregation is typically studied in the form of standing clusters without rotation (Muller and Held 2012; Wing and Emanuel 2014; Yang 2018) or cyclones on an *f* plane (Muller and Romps 2018; Wing et al. 2016) in idealized models. In the real world, one example of convective aggregation is the tropical cyclone (TC). The role of radiation in TC development has been highlighted in recent studies. For example, using an idealized model, Smith et al. (2020) showed that radiation primarily accelerates tropical cyclone genesis by moistening the core of a disturbance. Also, recent studies on Hurricane Edouard found that radiative cooling plays an important role in its formation and intensification (Tang and Zhang 2016; Tang et al. 2019). Using a convection-resolving model, Ruppert et al. (2020) showed that cloud radiative feedback promotes and accelerates TC evolution in the context of Typhoon Haiyan and Hurricane Maria. From a climatological perspective, it remains unclear how radiation affects TC development in GCMs with spatially varying boundary conditions. GCMs can simulate TCs with horizontal grid spacings of ~100–200 km (Broccoli and Manabe 1990; Knutson et al. 2010). However, TCs simulated at such coarse resolution exhibit significant biases such as weaker intensity and larger size compared to observations (Camargo et al. 2020; Walsh et al. 2007, 2015). Recently, high-resolution models have demonstrated significant progress in simulating TCs (Murakami et al. 2017a,b, 2018; Vecchi et al. 2019; Wehner et al. 2015; Zhao et al. 2009), which provides a platform where the impact of radiative feedbacks on TCs can be examined under realistic background conditions.

In this study, we use a high-resolution and TC-permitting GCM to assess the response of TCs when total radiative cooling rates (longwave plus shortwave) are fixed with climatological values. Instead of completely removing the CRE, we suppress synoptic-scale radiative interactions by prescribing total radiative cooling rates (longwave plus shortwave) using their monthly climatological values. Various numerical simulations are performed in the present-day climate as well as under different idealized global warming scenarios. It is found that suppressing radiative interactions reduces not only global TC frequency but also TC duration in the present-day climate. However, the magnitude of reduction in TC frequency is shown to be sensitive to different warming scenarios. We also do experiments prescribed with interannually varying SSTs and compare them with observations to verify the robustness of our results.

2. Methods

a. Model and experiments

In this study, the High-Resolution Atmospheric Model (HiRAM) developed at the Geophysical Fluid Dynamics Laboratory (GFDL) is used to investigate the impact of radiative interactions on TCs. HiRAM has a horizontal grid spacing of ~50 km and can successfully reproduce the observed global TC climatology and interannual variability (Zhao et al. 2009).

We first perform two simulations with prescribed climatological monthly means of SSTs and sea ice from the Hadley Centre Sea Ice and Sea Surface Temperature (HadISST) dataset (Rayner et al. 2003) based on the 20-yr period from 1986 to 2005. These two simulations are integrated for 50 years with a constant atmospheric CO_2 concentration (at 1990 levels). While one simulation (referred to as the Control run) follows the default model configuration and thus has fully interactive radiation, the other simulation (referred to as the

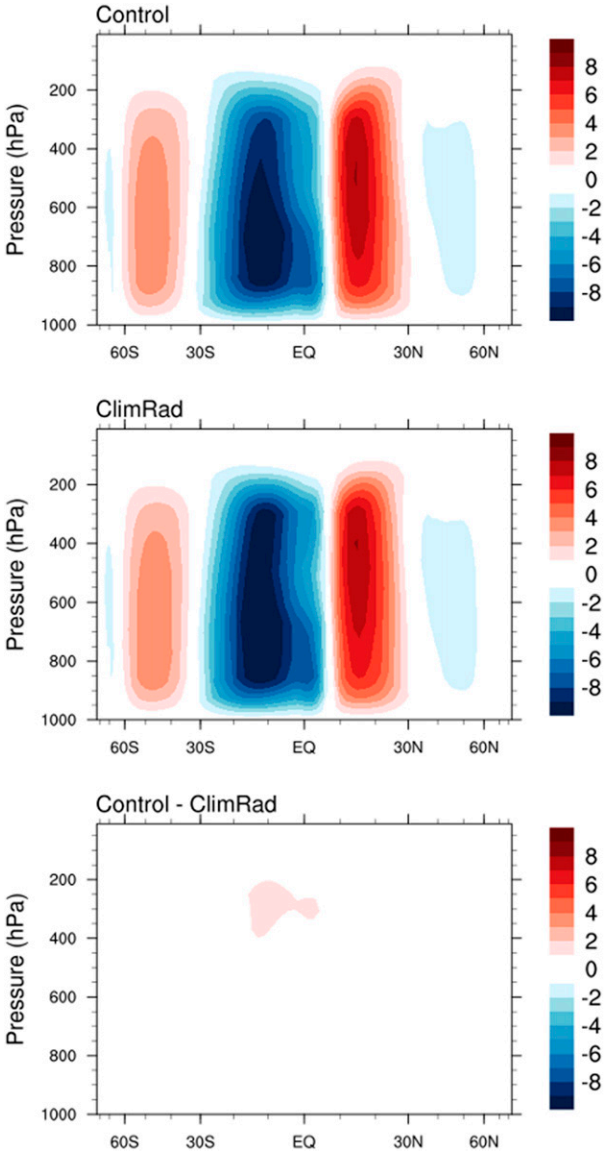

FIG. 1. Annual mean, zonal mean meridional circulation (unit: $\times 10^{10}$ kg s^{-1}) in the (top) Control run, (middle) ClimRad run, and (bottom) their difference.

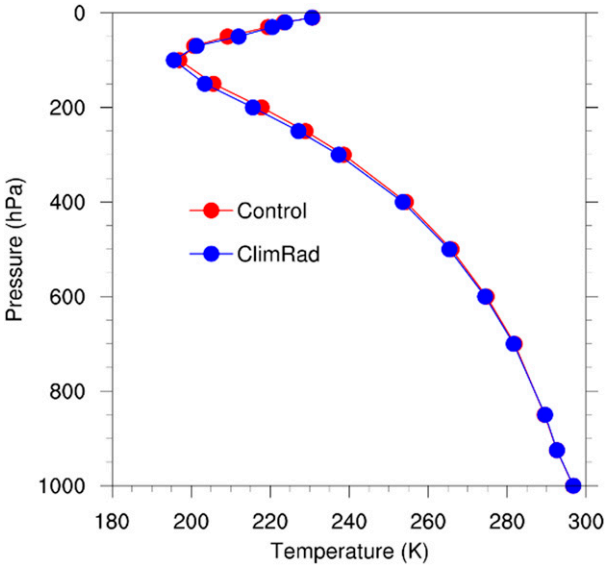

FIG. 2. Temperature profile averaged over the tropics for the Control run (red) and ClimRad run (blue).

ClimRad run) overwrites the model-generated atmospheric total radiative cooling rates (longwave plus shortwave) with their monthly varying climatological values computed from the Control run. Specifically, the overwriting process is implemented as follows: (i) monthly atmospheric total radiative cooling rates are retrieved from the last 20 years of the Control run; (ii) a multiyear average is applied to the 20-yr data to get monthly varying climatological radiative cooling rates; and (iii) each time when the radiation code is called in the ClimRad run, the atmospheric radiative cooling rates are overwritten by its monthly varying climatological values that are temporally interpolated to the current time step. These two simulations aim at assessing the impact of suppressing radiative interactions on TCs in the present-day climate. We note that the ClimRad run is different from the simulations in the COOKIE project. While removing the CRE results in substantial changes in the mean state (Li et al. 2015), the overwriting approach keeps the mean state almost unchanged. For example, the zonal mean meridional overturning circulation exhibits little difference between the Control and ClimRad runs (Fig. 1). Also, the temperature profiles averaged over the tropics (30°S–30°N) in these two runs are almost identical to each other (Fig. 2), indicating that the lapse rate is hardly affected by the overwriting approach.

Additional simulations are performed to explore how suppressing radiative interactions affects the development of TCs in a warmer climate. In this study, we have three warming scenarios: 1) adding a uniform 4 K warming to the observed multiyear average SSTs (referred to as plus4K); 2) adding a uniform 2 K warming to the observed multiyear average SSTs and doubling CO_2 concentration (referred to as plus2K_2×CO_2); 3) doubling CO_2 concentration only (referred to as 2×CO_2). While the number 2 scenario could be more realistic, together these simulations aim at comparing the relative importance of radiative interactions in different idealized warming scenarios. The control experiments used in this study are described in Hsieh et al. (2020). There are two simulations in each warming scenario: one with fully interactive radiation while the other is prescribed with monthly varying radiative cooling rates computed from the simulation with interactive radiation. For example, monthly varying radiative cooling rates used in the ClimRad_plus4K run are computed from the Control_plus4K run. By doing this, the two simulations in each scenario have the same mean values of radiative cooling rates. Table 1 summarizes these simulations.

b. *Tracking tropical cyclones*

TCs simulated in HiRAM are identified using the tracker developed by Harris et al. (2016). This method uses instantaneous 6-hourly outputs of sea level pressure, midtropospheric temperature, 850 hPa vorticity, and 10 m zonal and meridional winds to track high cyclonic vorticity features. Typically, the high cyclonic vorticity is accompanied with a sea level pressure minimum, a warm core in the middle troposphere and strong near-surface winds. We note that the parameters used here are slightly different from those in Murakami et al. (2016). The minimum wind speed criterion is set at 15.3 m s^{-1}, which is based on the suggestions of Walsh et al. (2007) of a threshold 10% below gale force (17 m s^{-1}) for a ~50 km resolution model. The minimum warm core temperature anomaly relative to the surrounding environment is set at 2.5 K to yield comparable global-mean TC frequency as observations. We note

TABLE 1. A list of the simulations conducted in this study.

Experiment name	SST forcing	CO_2 forcing	Radiation
Control	1986–2005 average	Fixed	Fully interactive
ClimRad	1986–2005 average	Fixed	Prescribed climatology
Control_plus4K	Add 4 K warming	Fixed	Fully interactive
ClimRad_plus4K	Add 4 K warming	Fixed	Prescribed climatology
Control_plus2K_2×CO_2	Add 2 K warming	2 × CO_2	Fully interactive
ClimRad_plus2K_2×CO_2	Add 2 K warming	2 × CO_2	Prescribed climatology
Control_2×CO_2	1986–2005 average	2 × CO_2	Fully interactive
ClimRad_2×CO_2	1986–2005 average	2 × CO_2	Prescribed climatology
Control-AMIP	1980–2017	Fixed	Fully interactive
ClimRad-AMIP	1980–2017	Fixed	Prescribed climatology

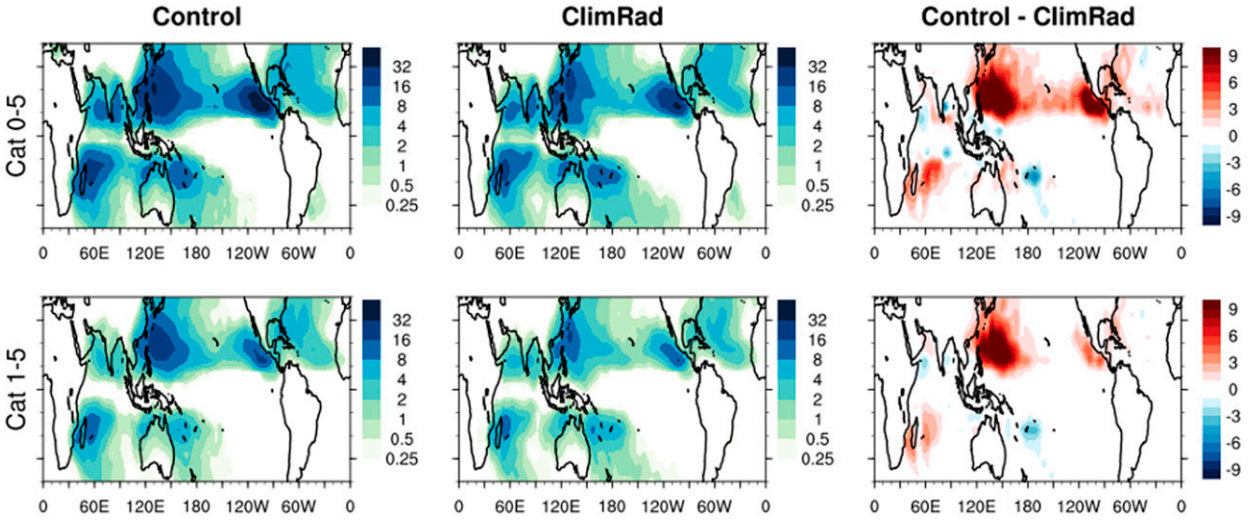

FIG. 3. Maps of track density per year for (top) category 0–5 and (bottom) category 1–5 TCs. Track density is defined by counting the total number of TCs in each 5° × 5° box. Results are from the (left) Control run, (center) ClimRad run, and (right) their difference.

that the main results of this study are not sensitive to the modest modifications of the tracking parameters used in this study.

3. Results

a. Global TC frequency

The role of radiative interactions is first examined in the present-day climate. Figure 3 shows maps of track density per year for tropical storm (category 0) through category 5 hurricanes (top) and category 1–5 TCs (bottom) computed from the Control run (left), ClimRad run (middle), and their difference (right). TCs are categorized based on the Saffir–Simpson scale. Track density is defined by counting the total number of TCs in each 5° × 5° box. When radiative interactions are suppressed there are substantial differences in the spatial distribution of track density. Overall, the track density in the ClimRad run becomes much lower than that in the Control run, indicating reduced TC activity when synoptic-scale radiative interactions are suppressed. In addition, the reduction in track density exhibits spatial heterogeneity, with the largest reduction over the northwest Pacific relative to other ocean basins.

The global number of TCs per year in the ClimRad run (blue boxes in Fig. 4) is smaller than that in the Control run (red boxes in Fig. 4). Each box represents the lower, median, and upper quartile of the global number of TCs per year and whiskers extend to points that lie within 1.5 interquartile range of the lower and upper quartile. We note that the Control and the ClimRad runs are forced by climatological SSTs based on 1986 through 2005, and the mean value of the number of TCs per year in the Control run is slightly different from observations. However, TCs in the Control and the ClimRad runs are tracked using the same tracking method with identical parameters. Compared to the Control run, the global number of TCs per year in the ClimRad run decreases by ~20% for both category 0–5 and category 1–5 TCs (Table 2). Global TC frequency is significantly reduced when synoptic-scale radiative interactions are suppressed.

In idealized models, previous studies have shown that the state of aggregation over a limited domain is binary, which means either a convectively aggregated state with one or several convective clusters, or a disaggregated state with disorganized convection (Bretherton et al. 2005; Muller and Held 2012; Wing and Emanuel 2014; Yang 2018). Under realistic boundary conditions, convectively aggregated systems such as TCs can still be simulated but happen less frequently without

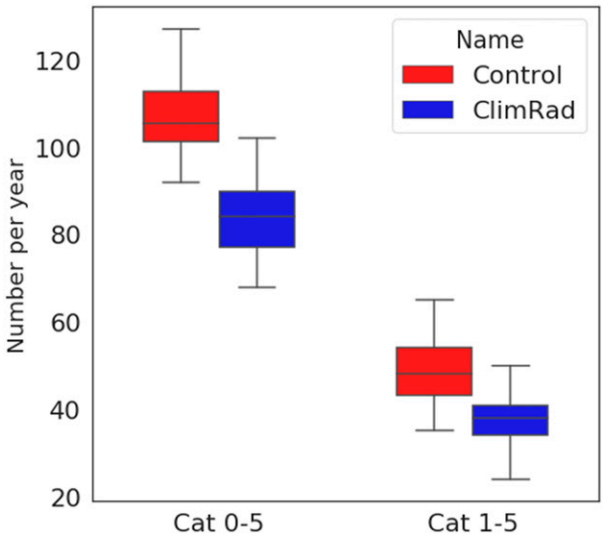

FIG. 4. Boxplots of the global number of TCs per year for category 0–5 and category 1–5 TCs for the Control run (red) and ClimRad run (blue). Student's *t* test shows that the difference in the number of TCs per year between the Control and ClimRad run is significant at 95% confidence level.

TABLE 2. Fractional change (%) in the global number of TCs when radiative interactions are suppressed.

	1986–2005 average	plus4K	plus2K_2×CO_2	2×CO_2
Category 0–5	22.0	17.3	18.6	21.8
Category 1–5	23.0	10.6	14.7	24.5

radiative interactions. This raises several questions: (i) Why does suppressing radiative interactions only reduce global TC frequency rather than preventing its occurrence completely in this GCM? (ii) What determines the magnitude of the reduction? Previous studies have suggested that without radiative feedback, numerical models are still capable of simulating typical TCs (Ooyama 1969; Rotunno and Emanuel 1987; Rotunno et al. 2009; Wing et al. 2016). Here the comparison between the Control run and the ClimRad run further confirms that TCs can be simulated in the complete absence of radiative interactions under realistic boundary conditions. Regarding (ii), recently Vecchi et al. (2019) and Hsieh et al. (2020) suggested that changes in TC frequency can be understood using a simple binomial model, where the TC frequency itself depends on the product of the number of TC seeds and the probability of these seeds successfully transforming into TCs. Thus, the fractional change in the expected value of TC frequency (n) is given by

$$\frac{\Delta n}{n} = \frac{\Delta N}{N} + \frac{\Delta p}{p}, \tag{1}$$

where N is the expected value of the frequency of TC seeds and p is the expected value of the probability of genesis of each seed. The seeds are defined as all tracks with 850 hPa vorticity of at least $1.5 \times 10^{-4}\,s^{-1}$ (negative in the Southern Hemisphere) and last for at least 12 h over the ocean surface in the tropics. Here p is inferred from the ventilation index of Tang and Emanuel (2012). The ventilation index (Λ) is defined as

$$\Lambda = \frac{u_{\text{shear}}\chi_{\text{entropy}}}{\text{PI}}, \tag{2}$$

where u_{shear} is the 850–200 hPa vertical wind shear, χ_{entropy} is the entropy deficit computed based on Tang and Emanuel (2012), and PI is potential intensity defined in Bister and Emanuel (1998). In this study, we define p as

$$p = \frac{0.02}{0.02 + \Lambda}. \tag{3}$$

We note that this definition is slightly different from Vecchi et al. (2019). Here, the constants in p are calculated to ensure that the product of the number of seeds and p best matches the number of TCs in the Control run. However, it remains consistent that large values of p mean high probability of TC genesis as in Vecchi et al. (2019) since large values of Λ means unfavorable conditions for TC genesis. By analyzing the response of TCs to doubling CO_2 in several GCMs, Vecchi et al. (2019) showed that the fractional change in global TC frequency can be explained by the combined effects of seeds and probability. More details of this theory can be found in Vecchi et al. (2019). The same framework (seeds and p) is then applied to the ClimRad run. When radiative interactions are suppressed, we find that the global probability of genesis increases by ~2%, whereas the frequency of TC seeds (i.e., pre-TC synoptic disturbances) decreases by ~20%. As a result, the change in TC frequency is expected to decrease by ~18%. This value is very close to the actual value of the fractional change in TC frequency (~20%) shown in Table 2, indicating that the reduction in TC activity is primarily due to the decrease in pre-TC synoptic disturbances.

Analyzing the energetics of TCs can provide a mechanistic perspective on the sensitivity of TCs to radiative decoupling. Previous studies have used an MSE budget analysis to quantify physical processes associated with convective aggregation (Bretherton et al. 2005; Muller and Bony 2015; Muller and Held 2012; Wing and Emanuel 2014; Wing et al. 2016; Wing et al. 2019). MSE (Neelin and Held 1987) is defined as

$$h = c_p T + gz + L_v q, \tag{4}$$

where c_p is the specific heat of dry air, T is the air temperature, g is the gravitational acceleration, z is the height above the surface, L_v is the latent heat of vaporization, and q is the specific humidity. The budget for the density-weighted vertical integral of MSE (denoted as $\hat{h}$) is computed as

$$\frac{\partial \hat{h}}{\partial t} = \text{THF} + R - \nabla_h \cdot \widehat{\mathbf{v}h}, \tag{5}$$

where THF is the surface turbulent heat flux including latent and sensible heat flux, R is net radiation of the atmosphere including both shortwave and longwave components, and $\nabla_h \cdot \widehat{\mathbf{v}h}$ is the horizontal divergence of the density-weighted vertical integral of the flux of h. The budget for the spatial variance of $\hat{h}$ is

$$\frac{1}{2}\frac{\partial \hat{h}^2}{\partial t} = \hat{h} \times \text{THF} + \hat{h} \times R - \hat{h} \times (\nabla_h \cdot \widehat{\mathbf{v}h}) \tag{6}$$

Usually, anomalies are computed for the variables in the above equation. For example, $\hat{h}'$ represents the density-weighted vertical integral of MSE anomaly. Using this framework, Wing et al. (2019) showed that the radiative feedback ($\hat{h}' \times R'$) contributes to the development of TCs, especially during early stage, while the surface flux feedback ($\hat{h}' \times \text{THF}'$) is stronger for more intense TCs.

Here we use a similar framework to compare the radiative feedback and the surface flux feedback in the development of TCs. Both terms are computed within a ~5° × 5° box centered on the tracked TCs. Anomalies are defined as the difference between the actual value at each grid point and its domain average of the ~5° × 5° box. In the tropics, horizontal

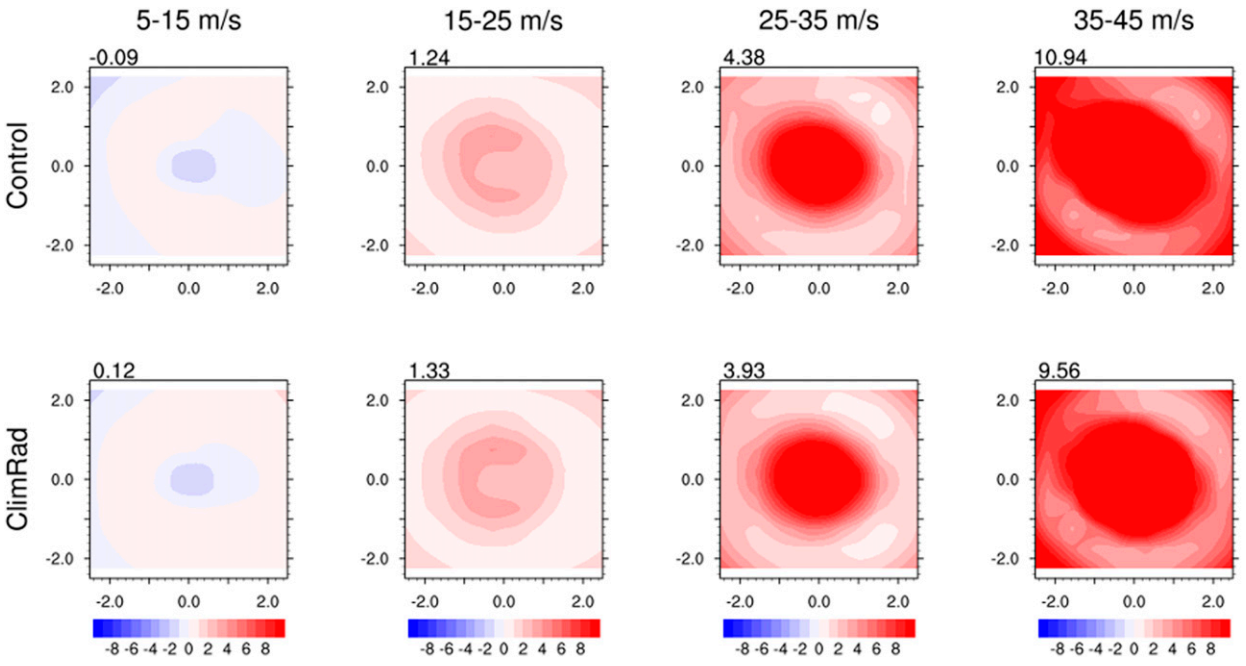

FIG. 5. Composites of $L_v\hat{q}' \times \mathrm{THF}'$ (unit: $\times 10^8\ \mathrm{J\ m^{-4}\ s^{-1}}$) for the (top) Control run and (bottom) ClimRad run during different TC stages: (left to right) 5–15, 15–25, 25–35, and 35–45 m s^{-1}. Domain average value is listed on the top left of each subplot.

temperature gradients are small. Variability of the vertical integral of water vapor is closely related to that of MSE (Muller and Romps 2018). Wing et al. (2019) discussed the vertical integral of MSE for TC-related analysis in high-resolution climate models. One way of computing MSE budget is to use column integral per column mass, but this approach is technically challenging as they argued and therefore not practical. The second way is to perform the column integral between two fixed pressure levels as they did in that paper, in which they chose 920 hPa as the lower boundary. However, the pressure is different at different wind speeds and there is horizontal gradient from the TC center outwards. Therefore, we use the product of the column-integrated water vapor (which is a direct model output from the surface to the top of atmosphere, denoted as $\hat{q}'$) and L_v to represent $\hat{h}'$, and compare $L_v\hat{q}' \times THF'$ and $L_v\hat{q}' \times R'$ in the Control run and the ClimRad run. Thereafter, the radiative feedback and the surface flux feedback are estimated by

$$\hat{h}' \times R' \approx L_v\hat{q}' \times R', \tag{7}$$

$$\hat{h}' \times THF' \approx L_v\hat{q}' \times THF'. \tag{8}$$

Figure 5 shows composites of $L_v\hat{q}' \times THF'$ during different TC stages from the 5–15 m s^{-1} bin to the 35–45 m s^{-1} bin. As TCs get stronger, the surface flux feedback increases no matter whether radiative interactions are suppressed. Additionally, both runs exhibit similar amplitude of $L_v\hat{q}' \times \mathrm{THF}'$ for the same bin, indicating that the surface flux feedback still contributes to the development of TCs without radiative interactions and its amplitude increases monotonically with TC intensity.

However, we find that contribution from the radiative feedback is very different. In Fig. 6, although the amplitude of $L_v\hat{q}' \times R'$ does not monotonically increase as TCs get stronger in the Control run, it is dominant at low wind speeds and then becomes approximately of the same order of magnitude as $L_v\hat{q}' \times THF'$ except for the strong wind bins (where wind speeds are greater than ~25 m s^{-1}). A further decomposition of the total radiative feedback into longwave and shortwave components indicates that the longwave radiative feedback contributes more than the shortwave radiative feedback (Figs. S1 and S2 in the online supplemental material). In the ClimRad run, $L_v\hat{q}' \times R'$ is almost zero through all bins, which means that with suppressed radiative–convective interactions, there is little contribution from the radiative feedback to the development of TCs. We repeat the above analysis using different box sizes for ~7° × 7° and ~9° × 9° boxes. The results are consistent with each other (not shown). In the 5–15 m s^{-1} bin, $L_v\hat{q}' \times THF'$ is negative near TC center in both runs, indicating that the surface flux feedback works against the development of TCs (Fig. 5). It is the positive radiative feedback ($L_v\hat{q}' \times R'$) in the Control run that promotes the TC development (Fig. 6). Since such positive contribution is missing in the ClimRad run, the amplitude of the combined effects of the surface flux feedback and the radiative feedback is smaller without radiative interactions (Fig. 7), resulting in less active TC activity. Previous studies using cloud-resolving models have shown that the surface flux feedback is overall positive during the development of TCs, even in the early stages (Muller and Romps 2018; Wing et al. 2016). In this GCM, although the amplitude of the surface flux feedback increases monotonically with TC intensity (i.e., the wind speed), its sign changes: being positive at high wind speeds

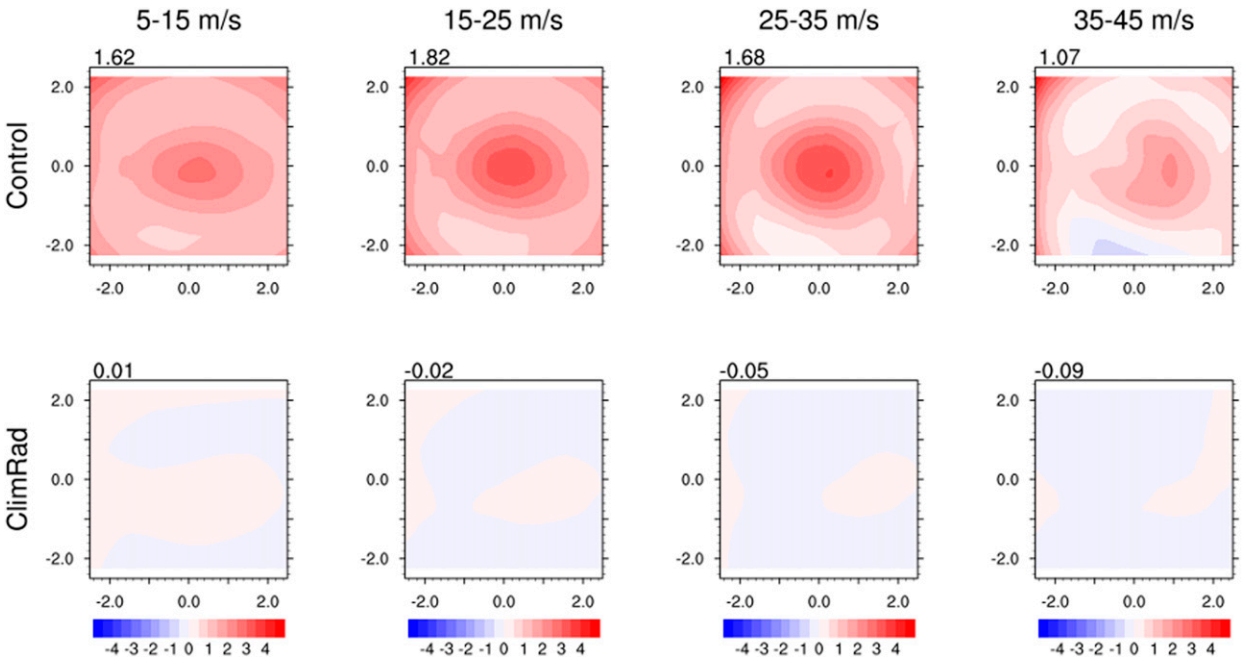

FIG. 6. As in Fig. 5, but for composites of $L_v\hat{q}' \times R'$ (unit: $\times 10^8\,\mathrm{J^2\,m^{-4}\,s^{-1}}$).

but negative at very low wind speeds. On one hand, it may be more accurate that the surface fluxes are resolved explicitly in idealized models. On the other, it could also reflect changes that, at low wind speeds, the air–sea enthalpy disequilibrium, which is a negative feedback, dominates the surface flux feedback because there is little impact of winds on enhancing the surface flux feedback (Wing and Emanuel 2014). More research is needed to address such discrepancy using higher-resolution GCMs in the future.

b. TC duration and genesis

To compare the distribution of TC duration with and without radiative interactions, the probability distribution function (PDF) of TC duration retrieved from the Control run is used to

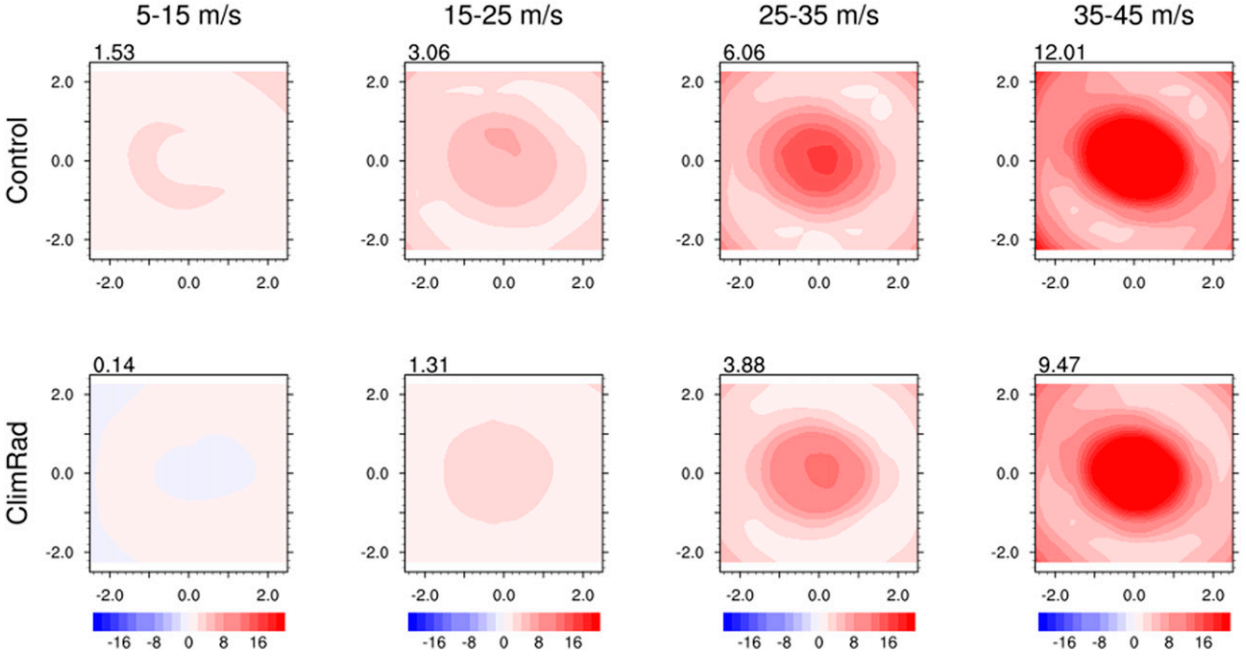

FIG. 7. As in Fig. 5, but for composites of the sum of $L_v\hat{q}' \times \mathrm{THF}'$ and $L_v\hat{q}' \times R'$ (unit: $\times 10^8\,\mathrm{J^2\,m^{-4}\,s^{-1}}$).

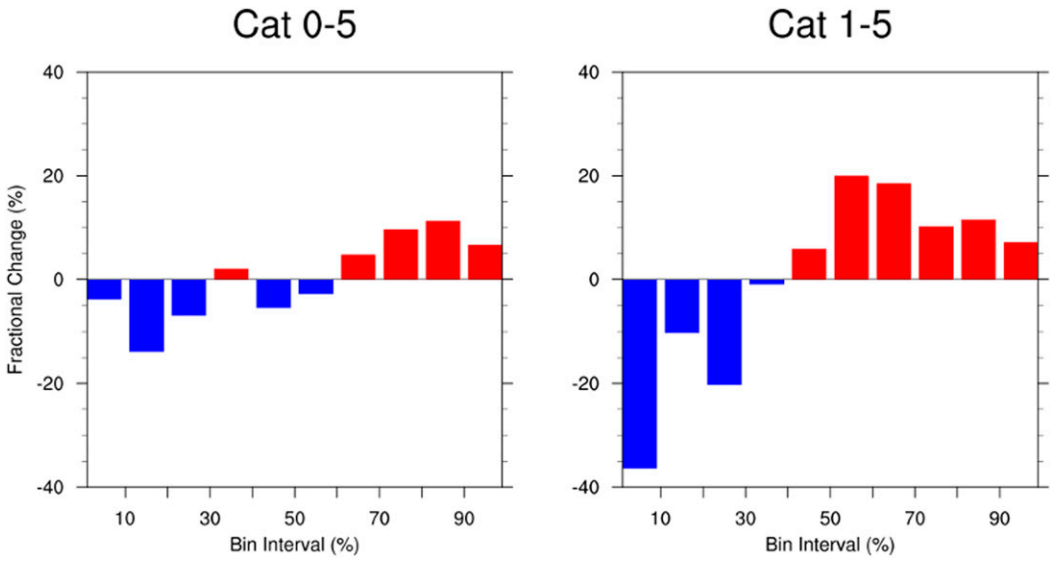

FIG. 8. Distribution of the fractional change in TC duration for (left) category 0–5 and (right) category 1–5 TCs in deciles. Large (small) bins mean long-lived (short lived) TCs. See text in section 3b for more details.

define duration deciles, where each decile contains 10% of the total number of TCs (note that the lowest and highest bins are unbounded below and above, respectively). With the lower and upper boundaries of each decile determined, TC duration retrieved from the ClimRad run is put into these deciles to produce another PDF. In each decile, the fractional change between the Control run and ClimRad run is computed. If more (less) cases are from the Control run in a decile, a positive (negative) fractional change is obtained. As TC duration increases, the fractional change switches from negative to positive for both category 0–5 and category 1–5 TCs (Fig. 8). These patterns indicate that the ClimRad run yields more short-lived and fewer long-lived TCs than the Control run. Taken as a whole, TC duration is reduced when radiative interactions are suppressed.

The reduction in TC duration can be understood by the differentiated response of TC genesis and lysis. Here genesis is defined as the location where the TC wind speed at 10 m first exceeds 17 m s^{-1} and has a warm core, while lysis is the location where the wind speed at 10 m last exceeds 17 m s^{-1} and the warm core disappears. We note that genesis and lysis density are normalized by the number of TCs per year in each simulation because the global TC frequency is different with and without radiative interactions. Figure 9 displays the normalized genesis density for category 0–5 and category 1–5 TCs in the Control run (left), ClimRad run (middle), and

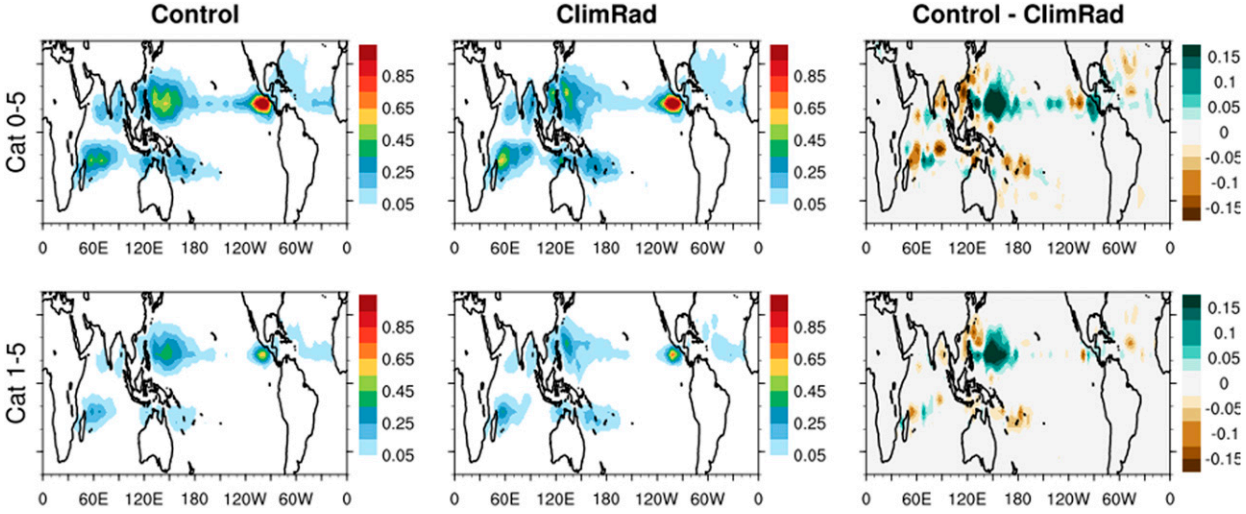

FIG. 9. Maps of the normalized genesis density for (top) category 0–5 and (bottom) category 1–5 TCs. Results are from the (left) Control run, (center) ClimRad run, and (right) their difference. See text in section 3b for more details.

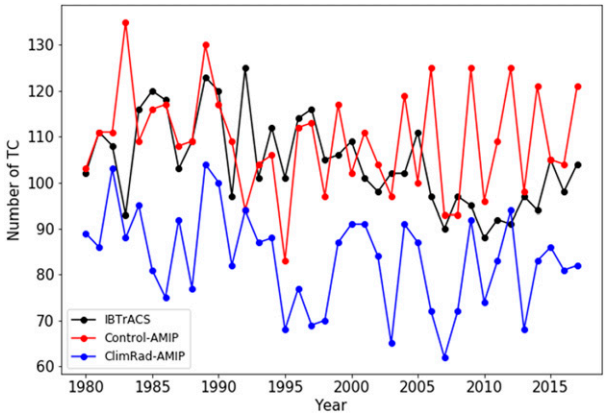

FIG. 10. Time series of the global number of TCs per year for the Control-AMIP (red line), ClimRad-AMIP (blue line), and IBTrACS (black line) from 1980 to 2017.

their difference (right). Without radiative interactions, genesis locations shift toward coastal regions, whereas TC lysis exhibits little difference (not shown). The response in genesis and lysis indicates that TCs are forming late in general, and thus have shorter lifetimes before reaching their natural lysis locations such as cold water, land, or regions with high wind shear, which leads to the reduction in TC duration as shown in Fig. 8. Thus, suppressing radiative interactions not only reduces TC genesis, but also delays genesis for those TCs that do develop. This delay in TC genesis is consistent with the reduction in contribution to the spatial variance of MSE in the ClimRad run (Fig. 7). Since $L_v\hat{q}' \times \mathrm{THF}'$ is a sink of spatial variance of MSE in the early stages of TC development (Fig. 5), $L_v\hat{q}' \times R'$ is crucial in promoting the development of TC (Fig. 6). The combined contribution is deficient in the ClimRad run compared to that in the Control run (Fig. 7). For those seeds that do develop into TCs, a longer time is required for them to accumulate energy without the contribution from the radiative feedback. At the same time, these seeds are moving toward land. The more time they spend in accumulating energy, the closer they get to land. This explains why TC genesis locations shift toward coastal regions.

c. *Simulations with interannually varying SSTs*

To verify the robustness of our results, two more simulations are performed by prescribing interannually varying SSTs from 1980 to 2017, which are similar to the Atmospheric Model Intercomparison Project (AMIP) that is part of phase 5 of the Coupled Model Intercomparison Project (CMIP5; Taylor et al. 2012). These two simulations are referred to as the Control-AMIP with interactive radiative cooling and the ClimRad-AMIP with suppressed radiative interactions. The number of TCs per year retrieved from these two AMIP-like simulations is compared to that retrieved from the International Best Track Archive for Climate Stewardship (Knapp et al. 2010), version 4 (IBTrACS v04). Figure 10 shows the time series of the number of TCs in each year for the Control-AMIP, the ClimRad-AMIP, and IBTrACS v04. While the number of TCs in the Control-AMIP and that in IBTrACS v04 are generally of the same level, the number of TCs in the ClimRad-AMIP is smaller, indicating that suppressing radiative interactions also reduces TC frequency with interannually varying SSTs.

d. *Sensitivity to background warming*

In this section, we explore how the change in TC activity due to suppressed radiative interactions depends on the mean state of the climate. To compare the change in TC activity in the present-day climate with that in a warmer climate, ΔTC is first defined to quantify the *difference* in track density between the Control run and the ClimRad run. Likewise, $\Delta\mathrm{TC}_{\mathrm{plus4K}}$, $\Delta\mathrm{TC}_{\mathrm{plus2K\_2\times CO_2}}$, and $\Delta\mathrm{TC}_{2\times\mathrm{CO_2}}$ represent such differences in each warming scenario respectively (details of each warming

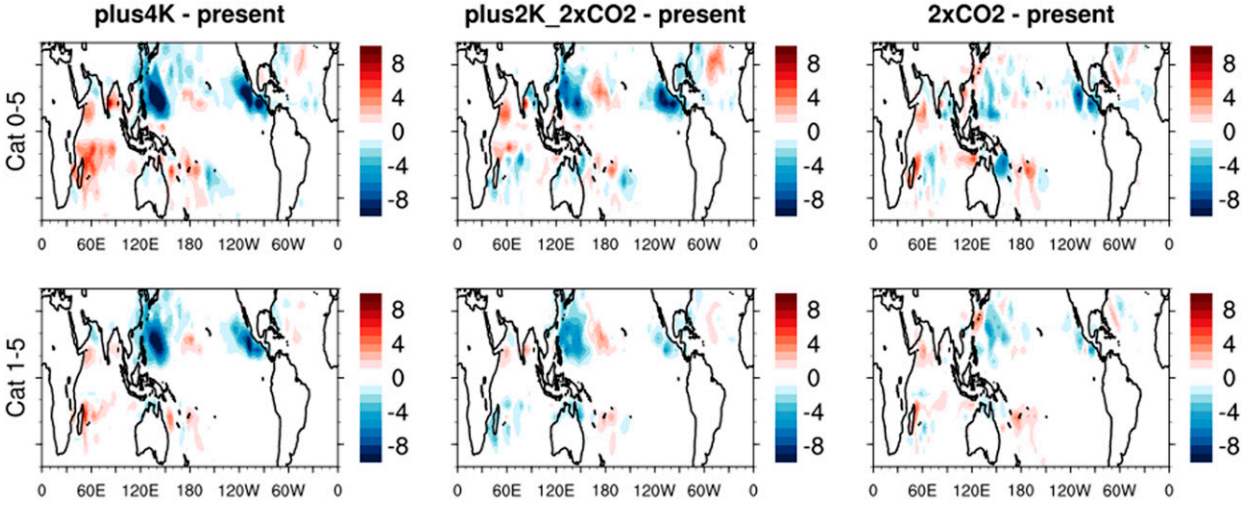

FIG. 11. Maps of (left) $\Delta\mathrm{TC}_{\mathrm{plus4K}} - \Delta\mathrm{TC}$, (center) $\Delta\mathrm{TC}_{\mathrm{plus2K\_2\times CO_2}} - \Delta\mathrm{TC}$, and (right) $\Delta\mathrm{TC}_{2\times\mathrm{CO_2}} - \Delta\mathrm{TC}$ for (top) category 0–5 and (bottom) category 1–5 TCs. ΔTC means the difference in track density in the present-day climate. See text in section 3d for more details.

scenario can be found in section 2). Then $\Delta TC_{plus4K} - \Delta TC$, $\Delta TC_{plus2K\_2\times CO_2} - \Delta TC$, and $\Delta TC_{2\times CO_2} - \Delta TC$ are computed to compare the change in track density due to suppressed radiative interactions in each warming scenario with that in the present-day climate. Figure 11 compares maps of $\Delta TC_{plus4K} - \Delta TC$, $\Delta TC_{plus2K\_2\times CO_2} - \Delta TC$, and $\Delta TC_{2\times CO_2} - \Delta TC$ for category 0–5 and category 1–5 TCs. While there are variations in the magnitude, the spatial patterns are similar. Negative values are found over the northwest and northeast Pacific, indicating that the magnitude of reduction in TC frequency due to suppressed radiative interactions is diminished in a warmer climate.

For the global number of TCs, the fractional change in the present-day climate is 22.0% (23.0%) for category 0–5 (category 1–5) TCs, whereas it becomes 17.3% (10.6%) in plus4K and 18.6% (14.7%) in plus2K_2×CO_2 (Table 2). The differences in the number of TCs with and without radiative interactions are statistically significant at 95% confidence level based on Student's *t* test. In Fig. 12, the global number of TCs per year in each warming scenario is normalized by the median value in its present-day counterpart. For example, the number in the Control_plus4K run is normalized by that in the Control run, while the number in the ClimRad_plus4K run is normalized by that in the ClimRad run. Mean values of the blue boxes are greater than those of the red boxes for plus4K and plus2K_2×CO_2, indicating a smaller reduction of TCs due to suppressed radiative interactions in these two warming scenarios. However, the fractional change in 2×CO_2 is almost identical to that in the present-day climate (Table 2) and mean values of the blue boxes are slightly smaller than those of the red boxes in 2×CO_2 (Fig. 12). Recall that $\Delta TC_{2\times CO_2} - \Delta TC$ is also small in magnitude, these results indicate that doubling CO_2 alone does not offset the reduction in TC frequency due to suppressed radiative interactions as robustly as what other warming scenarios do.

Overall, there is an increase in latent heat release as climate warms (Held and Soden 2006), especially with increased SSTs, which contributes more energy to the development of TCs. Therefore, the impact of suppressing radiative interactions is less effective due to the greater relative contributions from latent heating. This can be quantified using the MSE budget analysis. Here, we compare the surface flux feedback and the radiative feedback in the present-day climate and the plus4K scenario. Compared to the Control run, the surface flux feedback and the radiative feedback increase in the Control_plus4K run (Fig. 13, top), so does the total feedback (Fig. 13, middle). However, the relative contributions of the surface flux feedback and the radiative feedback change as SSTs increase. In the Control run, the radiative feedback dominates over the surface flux feedback in early stages of TC development (Fig. 13, bottom left), whereas the relative contribution from the radiative feedback decreases in the Control_plus4K run with an increase in the relative contribution from the surface flux feedback (Fig. 13, bottom right). Thus, with increased SSTs, the radiative feedback contributes a smaller fraction to the spatial variance of MSE while the surface flux feedback plays a more important role in TC formation. Based on this, when the contribution from the radiative feedback is removed in ClimRad_plus4K, there is less reduction in TC frequency.

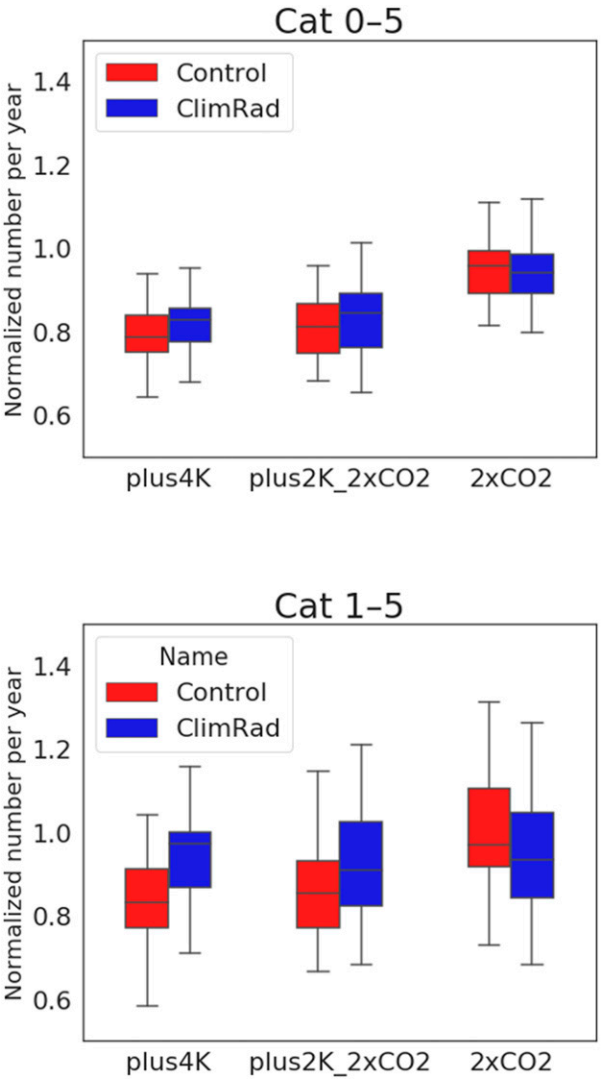

FIG. 12. Boxplots of the normalized global number of TCs per year for (top) category 0–5 and (bottom) category 1–5 (bottom) TCs in each warming scenario. Student's *t* test shows that the difference in the number of TCs per year between the Control and ClimRad run before normalization is significant at 95% confidence level in all warming scenarios.

4. Summary and discussion

In this study, we examine the impact of radiative interactions on the development of TCs under realistic boundary conditions. Unlike previous studies that completely remove cloud radiative effects, we only suppress the radiation variations on synoptic time scales by overwriting the model-generated atmospheric radiative cooling rates with its monthly varying climatological values. We find that suppressing radiative interactions reduces both TC frequency and TC duration in the present-day climate. While the reduction in TC frequency is primarily due to a decrease in the frequency of pre-TC synoptic disturbances, the reduction in TC duration arises from a delay

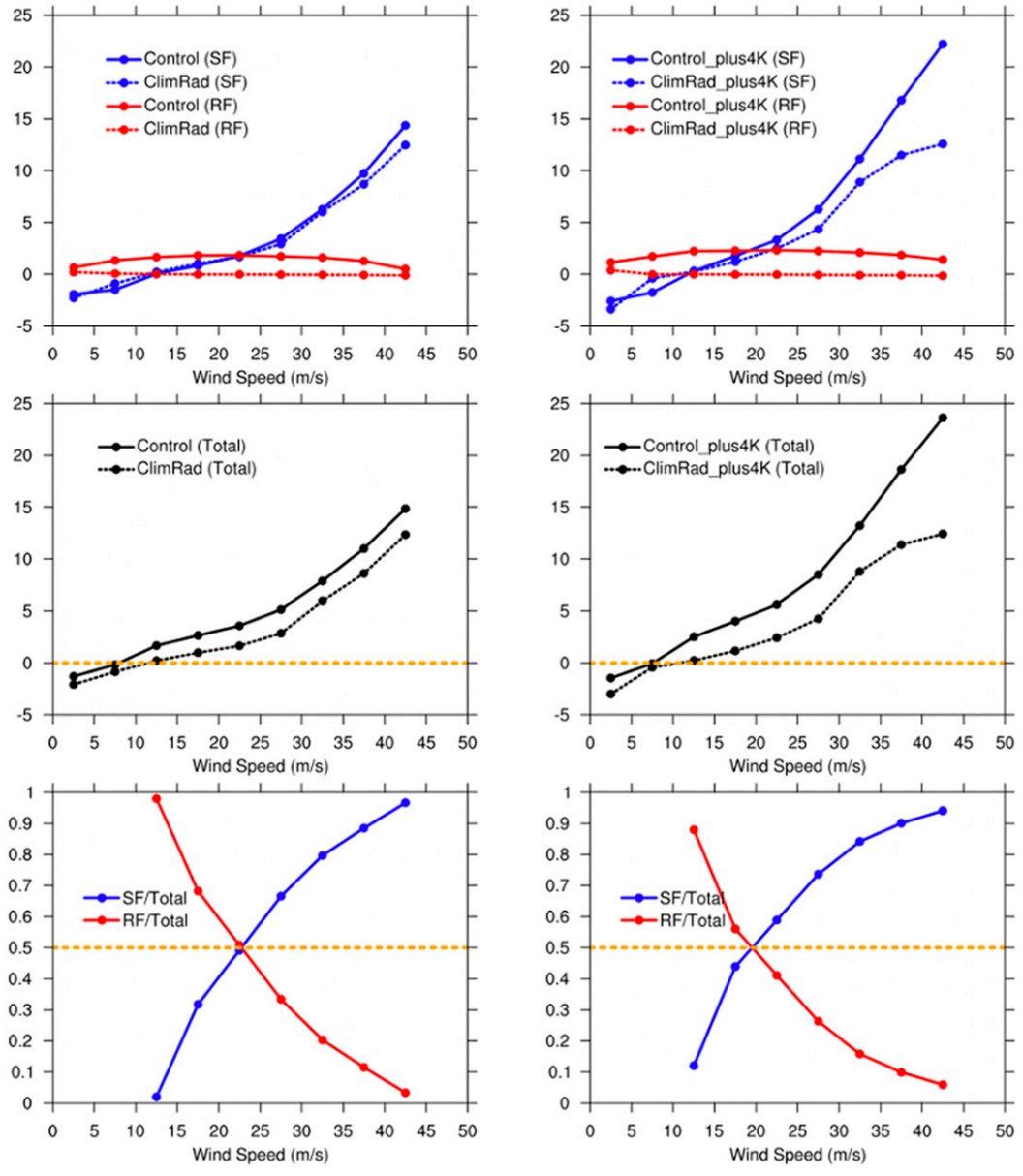

FIG. 13. (top) The surface flux feedback (SF; blue lines) and the radiative feedback (RF; red lines) in the (left) present-day climate and (right) plus4K scenario as a function of TC intensity in 5 m s^{-1} intervals. (middle) The sum of SF and RF. The (top) and (middle) rows have a unit of $\times 10^8$ J^2 m^{-4} s^{-1}. Simulations with (without) radiative interactions are marked with solid (dashed) lines. (bottom) The ratio of SF to the total feedback (blue solid lines) and the ratio of RF to the total feedback (red solid lines) in (left) the Control run and (right) the Control_plus4K run when both SF and RF become positive. Each variable is averaged over a ~5° × 5° box centered on the TC.

in genesis and resulting spatial shift of TC genesis locations toward coastal regions, with lysis locations remaining unchanged. Based on the MSE budget analysis, we show that although suppressing radiative interactions does not change the surface flux feedback, it greatly reduces the contribution from the radiative feedback to the development of TCs, explaining why TC frequency is reduced when radiative–convective coupling is disabled. While the surface flux feedback is negative at low wind speeds and thus inhibits the development of TC, the radiative feedback is positive and increases the spatial variance of MSE. Therefore, the radiative feedback plays a more important role in the early stages of TC development. We further explore the sensitivity of the impact of suppressing radiative interactions to the mean state of the climate. It is found that the impact of suppressing radiative interactions is diminished with increased SSTs, which likely reflects the greater role of latent heating in the warmer and more humid base state.

Additionally, we find that the change in TC frequency exhibits spatial heterogeneity. In the present-day climate, suppressing radiative interactions leads to a greater reduction in TC frequency over the western Pacific than the other basins (Figs. S3–S5). Previous studies have shown that processes like weak downdrafts below clouds (Muller and Bony 2015) or enhanced virtual effect (Yang 2018) can trigger convective aggregation without radiative–convective interactions in idealized models. More investigation is needed to explore the impact of these processes under realistic boundary conditions. Instead of removing CRE, this study suppresses radiative interactions by using climatological values of radiative cooling rates, looking both at cloud-induced and clear-sky effects in combination. Therefore, this study does not address whether and how clear-sky radiation affects TC development given that cloud-induced radiative perturbations have been found to be important to TC development (Bu et al. 2014; Muller and Romps 2018; Ruppert et al. 2020; Smith et al. 2020; Wing et al. 2016).

We note that the simulations in this study are performed with prescribed SSTs. Future studies may examine the impact of radiative interactions on TC development using fully coupled GCMs. The resolution of this model could be another factor that affects how TCs respond to suppressed radiative interactions. The horizontal grid spacing in HiRAM is ~50 km, which is still coarse for TC simulations although it can reproduce the observed global TC climatology quantitatively. Also, while GCMs use cumulus parameterization, our results are largely consistent with recent studies using convection-resolving models (Ruppert et al. 2020; Wing et al. 2016), which indicate that cumulus parameterization and horizontal grid spacing do not undermine the main conclusions in this study. Future studies can explore the role of radiative interactions in TC development using GCMs with finer horizontal grids.

Acknowledgments. We thank three anonymous reviewers for their valuable comments and suggestions. B. Z. thanks Enhui Liao for his help. This research was supported by NOAA Awards NA18OAR4310269, NA18OAR4310418, and NA20OAR4310393, and Department of Energy Award DE-SC0021333. HiRAM simulations are performed on the Princeton University Research Computing systems. The data sets produced in this study are available upon request.

REFERENCES

Bister, M., and K. A. Emanuel, 1998: Dissipative heating and hurricane intensity. *Meteor. Atmos. Phys.*, **65**, 233–240, https://doi.org/10.1007/BF01030791.

Bretherton, C. S., P. N. Blossey, and M. Khairoutdinov, 2005: An energy-balance analysis of deep convective self-aggregation above uniform SST. *J. Atmos. Sci.*, **62**, 4273–4292, https://doi.org/10.1175/JAS3614.1.

Broccoli, A., and S. Manabe, 1990: Can existing climate models be used to study anthropogenic changes in tropical cyclone climate? *Geophys. Res. Lett.*, **17**, 1917–1920, https://doi.org/10.1029/GL017i011p01917.

Bu, Y. P., R. G. Fovell, and K. L. Corbosiero, 2014: Influence of cloud–radiative forcing on tropical cyclone structure. *J. Atmos. Sci.*, **71**, 1644–1662, https://doi.org/10.1175/JAS-D-13-0265.1.

Camargo, S. J., and Coauthors, 2020: Characteristics of model tropical cyclone climatology and the large-scale environment. *J. Climate*, **33**, 4463–4487, https://doi.org/10.1175/JCLI-D-19-0500.1.

Crueger, T., and B. Stevens, 2015: The effect of atmospheric radiative heating by clouds on the Madden-Julian Oscillation. *J. Adv. Model. Earth Syst.*, **7**, 854–864, https://doi.org/10.1002/2015MS000434.

Emanuel, K., A. A. Wing, and E. M. Vincent, 2014: Radiative-convective instability. *J. Adv. Model. Earth Syst.*, **6**, 75–90, https://doi.org/10.1002/2013MS000270.

Fermepin, S., and S. Bony, 2014: Influence of low-cloud radiative effects on tropical circulation and precipitation. *J. Adv. Model. Earth Syst.*, **6**, 513–526, https://doi.org/10.1002/2013MS000288.

Harris, L. M., S.-J. Lin, and C. Tu, 2016: High-resolution climate simulations using GFDL HiRAM with a stretched global grid. *J. Climate*, **29**, 4293–4314, https://doi.org/10.1175/JCLI-D-15-0389.1.

Held, I. M., and B. J. Soden, 2006: Robust responses of the hydrological cycle to global warming. *J. Climate*, **19**, 5686–5699, https://doi.org/10.1175/JCLI3990.1.

Holloway, C. E., and S. J. Woolnough, 2016: The sensitivity of convective aggregation to diabatic processes in idealized radiative-convective equilibrium simulations. *J. Adv. Model. Earth Syst.*, **8**, 166–195, https://doi.org/10.1002/2015MS000511.

Hsieh, T.-L., G. A. Vecchi, W. Yang I. M. Held, and S. T. Garner, 2020: Large-scale control on the frequency of tropical cyclones and seeds: A consistent relationship across a hierarchy of global atmospheric models. *Climate Dyn.*, **55**, 3177–3196, https://doi.org/10.1007/s00382-020-05446-5.

Knapp, K. R., M. C. Kruk, D. H. Levinson, H. J. Diamond, and C. J. Neumann, 2010: The International Best Track Archive for Climate Stewardship (IBTrACS) unifying tropical cyclone data. *Bull. Amer. Meteor. Soc.*, **91**, 363–376, https://doi.org/10.1175/2009BAMS2755.1.

Knutson, T. R., and Coauthors, 2010: Tropical cyclones and climate change. *Nat. Geosci.*, **3**, 157–163, https://doi.org/10.1038/ngeo779.

Li, Y., D. W. Thompson, and S. Bony, 2015: The influence of atmospheric cloud radiative effects on the large-scale atmospheric circulation. *J. Climate*, **28**, 7263–7278, https://doi.org/10.1175/JCLI-D-14-00825.1.

Muller, C. J., and I. M. Held, 2012: Detailed investigation of the self-aggregation of convection in cloud-resolving simulations. *J. Atmos. Sci.*, **69**, 2551–2565, https://doi.org/10.1175/JAS-D-11-0257.1.

——, and S. Bony, 2015: What favors convective aggregation and why? *Geophys. Res. Lett.*, **42**, 5626–5634, https://doi.org/10.1002/2015GL064260.

——, and D. M. Romps, 2018: Acceleration of tropical cyclogenesis by self-aggregation feedbacks. *Proc. Natl. Acad. Sci. USA*, **115**, 2930–2935, https://doi.org/10.1073/pnas.1719967115.

Murakami, H., G. Villarini, G. A. Vecchi, W. Zhang, and R. Gudgel, 2016: Statistical–dynamical seasonal forecast of North Atlantic and U.S. landfalling tropical cyclones using the high-resolution GFDL FLOR coupled model. *Mon. Wea. Rev.*, **144**, 2101–2123, https://doi.org/10.1175/MWR-D-15-0308.1.

——, G. A. Vecchi, and S. Underwood, 2017a: Increasing frequency of extremely severe cyclonic storms over the Arabian Sea. *Nat. Climate Change*, **7**, 885–889, https://doi.org/10.1038/s41558-017-0008-6.

——, and Coauthors, 2017b: Dominant role of subtropical Pacific warming in extreme eastern Pacific hurricane seasons: 2015 and the future. *J. Climate*, **30**, 243–264, https://doi.org/10.1175/JCLI-D-16-0424.1.

——, E. Levin, T. Delworth, R. Gudgel, and P.-C. Hsu, 2018: Dominant effect of relative tropical Atlantic warming on major hurricane occurrence. *Science*, **362**, 794–799, https://doi.org/10.1126/science.aat6711.

Neelin, J. D., and I. M. Held, 1987: Modeling tropical convergence based on the moist static energy budget. *Mon. Wea. Rev.*, **115**, 3–12, https://doi.org/10.1175/1520-0493(1987)115<0003:MTCBOT>2.0.CO;2.

Ooyama, K., 1969: Numerical simulation of the life cycle of tropical cyclones. *J. Atmos. Sci.*, **26**, 3–40, https://doi.org/10.1175/1520-0469(1969)026<0003:NSOTLC>2.0.CO;2.

Randall, D. A., D. A. Dazlich, and T. G. Corsetti, 1989: Interactions among radiation, convection, and large-scale dynamics in a general circulation model. *J. Atmos. Sci.*, **46**, 1943–1970, https://doi.org/10.1175/1520-0469(1989)046<1943:IARCAL>2.0.CO;2.

Rayner, N., D. E. Parker, E. B. Horton, C. K. Folland, L. V. Alexander, D. P. Rowell, E. C. Kent, and A. Kaplan, 2003: Global analyses of sea surface temperature, sea ice, and night marine air temperature since the late nineteenth century. *J. Geophys. Res.*, **108**, 4407, https://doi.org/10.1029/2002JD002670.

Rotunno, R., and K. A. Emanuel, 1987: An air–sea interaction theory for tropical cyclones. Part II: Evolutionary study using a nonhydrostatic axisymmetric numerical model. *J. Atmos. Sci.*, **44**, 542–561, https://doi.org/10.1175/1520-0469(1987)044<0542:AAITFT>2.0.CO;2.

——, Y. Chen, W. Wang, C. Davis, J. Dudhia, and G. Holland, 2009: Large-eddy simulation of an idealized tropical cyclone. *Bull. Amer. Meteor. Soc.*, **90**, 1783–1788, https://doi.org/10.1175/2009BAMS2884.1.

Ruppert, J. H., A. A. Wing X. Tang, and E. L. Duran, 2020: The critical role of cloud–infrared radiation feedback in tropical cyclone development. *Proc. Natl. Acad. Sci. USA*, **117**, 27 884–27 892, https://doi.org/10.1073/pnas.2013584117.

Sherwood, S. C., V. Ramanathan, T. P. Barnett, M. K. Tyree, and E. Roeckner, 1994: Response of an atmospheric general circulation model to radiative forcing of tropical clouds. *J. Geophys. Res.*, **99**, 20 829–20 845, https://doi.org/10.1029/94JD01632.

Slingo, A., and J. Slingo, 1988: The response of a general circulation model to cloud longwave radiative forcing. I: Introduction and initial experiments. *Quart. J. Roy. Meteor. Soc.*, **114**, 1027–1062, https://doi.org/10.1002/qj.49711448209.

Smith, W. P., M. E. Nicholls, and R. A. Pielke Sr., 2020: The role of radiation in accelerating tropical cyclogenesis in idealized simulations. *J. Atmos. Sci.*, **77**, 1261–1277, https://doi.org/10.1175/JAS-D-19-0044.1.

Stevens, B., S. Bony, and M. Webb, 2012: Clouds On-Off Klimate Intercomparison Experiment (COOKIE). EUCLIPSE, 12 pp., http://www.euclipse.eu/downloads/Cookie.pdf.

Tang, B., and K. Emanuel, 2012: A ventilation index for tropical cyclones. *Bull. Amer. Meteor. Soc.*, **93**, 1901–1912, https://doi.org/10.1175/BAMS-D-11-00165.1.

Tang, X., and F. Zhang, 2016: Impacts of the diurnal radiation cycle on the formation, intensity, and structure of Hurricane Edouard (2014). *J. Atmos. Sci.*, **73**, 2871–2892, https://doi.org/10.1175/JAS-D-15-0283.1.

——, Z.-M. Tan, J. Fang, E. B. Munsell, and F. Zhang, 2019: Impact of the diurnal radiation contrast on the contraction of radius of maximum wind during intensification of Hurricane Edouard (2014). *J. Atmos. Sci.*, **76**, 421–432, https://doi.org/10.1175/JAS-D-18-0131.1.

Taylor, K. E., R. J. Stouffer, and G. A. Meehl, 2012: An overview of CMIP5 and the experiment design. *Bull. Amer. Meteor. Soc.*, **93**, 485–498, https://doi.org/10.1175/BAMS-D-11-00094.1.

Vecchi, G. A., and Coauthors, 2019: Tropical cyclone sensitivities to CO_2 doubling: Roles of atmospheric resolution, synoptic variability and background climate changes. *Climate Dyn.*, **53**, 5999–6033, https://doi.org/10.1007/s00382-019-04913-y.

Walsh, K. J. E., M. Fiorino, C. Landsea, and K. McInnes, 2007: Objectively determined resolution-dependent threshold criteria for the detection of tropical cyclones in climate models and reanalyses. *J. Climate*, **20**, 2307–2314, https://doi.org/10.1175/JCLI4074.1.

——, and Coauthors, 2015: Hurricanes and climate: The U.S. CLIVAR working group on hurricanes. *Bull. Amer. Meteor. Soc.*, **96**, 997–1017, https://doi.org/10.1175/BAMS-D-13-00242.1.

Wehner, M., K. A. Reed, D. Stone, W. D. Collins, and J. Bacmeister, 2015: Resolution dependence of future tropical cyclone projections of CAM5.1 in the U.S. CLIVAR Hurricane Working Group idealized configurations. *J. Climate*, **28**, 3905–3925, https://doi.org/10.1175/JCLI-D-14-00311.1.

Wing, A. A., and K. A. Emanuel, 2014: Physical mechanisms controlling self-aggregation of convection in idealized numerical modeling simulations. *J. Adv. Model. Earth Syst.*, **6**, 59–74, https://doi.org/10.1002/2013MS000269.

——, S. J. Camargo, and A. H. Sobel, 2016: Role of radiative–convective feedbacks in spontaneous tropical cyclogenesis in idealized numerical simulations. *J. Atmos. Sci.*, **73**, 2633–2642, https://doi.org/10.1175/JAS-D-15-0380.1.

——, and Coauthors, 2019: Moist static energy budget analysis of tropical cyclone intensification in high-resolution climate models. *J. Climate*, **32**, 6071–6095, https://doi.org/10.1175/JCLI-D-18-0599.1.

Yang, D., 2018: Boundary layer diabatic processes, the virtual effect, and convective self-aggregation. *J. Adv. Model. Earth Syst.*, **10**, 2163–2176, https://doi.org/10.1029/2017MS001261.

Zhao, M. I. M. Held, S.-J. Lin, and G. A. Vecchi, 2009: Simulations of global hurricane climatology, interannual variability, and response to global warming using a 50-km resolution GCM. *J. Climate*, **22**, 6653–6678, https://doi.org/10.1175/2009JCLI3049.1.